Journal of Science and Technology in Civil Engineering, HUCE, 2025, 19 (1): 119–130

ISOGEOMETRIC FREE VIBRATION OF THE POROUS METAL FOAM PLATES RESTING ON AN ELASTIC FOUNDATION USING A QUASI-3D REFINED THEORY

Trang Tan Trien[a], Le Thanh Phong[a], Pham Tan Hung[a,*]

[a]*Faculty of Civil Engineering, Ho Chi Minh City University of Technology and Education (HCMUTE), No. 1 Vo Van Ngan street, Linh Chieu ward, Thu Duc city, Ho Chi Minh city, Vietnam*

Article history:
Received 13/12/2024, Revised 17/01/2025, Accepted 18/3/2025

Abstract

This study investigates the free vibration behavior of porous metal foam plates using the Quasi-3D refined plate theory. We consider three types of pores across the plate thickness: uniform, symmetric, and asymmetric distributions. Besides, the metal foam plate is reinforced by a Winkler-Pasternak foundation. By employing the variational principle and Quasi-3D refined theory, we derive the weak form for free vibration analysis. The Quasi-3D theory is essential for analyzing plates, as it accurately captures transverse shear and normal deformations, which are vital for understanding the behavior of thick and moderately thick plates. Unlike simpler models, it provides a detailed representation of stress and strain distributions across the plate's thickness, enabling precise modeling of complex structural behaviors. The natural frequency of the porous metal foam plates is determined by solving the explicit governing equation using the isogeometric approach. Additionally, we examine how the porous coefficient, porous distribution, and geometry impact the vibrational frequency of the porous metal foam plate.

Keywords: quasi-3D refined theory; isogeometric approach; porous metal foam plates; porous distribution.

https://doi.org/10.31814/stce.huce2025-19(1)-10

1. Introduction

Porous structures have been the focus of intensive research in recent years due to their exceptional mechanical properties. Chen et al. [1] presented the nonlinear vibration of sandwich beams with a functionally graded (FG) porous metal foam core according to the Timoshenko beam theory. Jabbari et al. [2, 3] used the classical plate theory (CPT) and analytical methods to investigate porous metal foam plates' mechanical and thermal buckling. Besides, Barati and colleagues [4] conducted analytical free vibration and buckling behaviors of the FG piezoelectric porous plates. Keddouri [5] employed the refined plate theory (RPT) and analytical method to examine the impact of porous coefficient and porous distribution on the deflection and stresses of FG sandwich plates with porosities. In the study [6], the free vibration of the metal foam cylindrical shell was investigated using the analytical approach and FSDT. Rezaei et al. [7] determined the vibrational frequency of the FG plate made of porous materials based on the first-order shear deformation plate theory (FSDT) and analytical approach. The analytical nonlinear vibration of the metal foam circular cylindrical shells with graphene platelets (GPL) reinforcement was examined by Wang et al. [8] using Donnell nonlinear shell theory. Ebrahimi et al. [9] used the analytical method combined with the RPT to introduce the free vibration of the porous metal foam plate supported in an elastic foundation. Li et al. [10] employed the FSDT and generalized differential quadrature (GDQ) method to explore the free vibration behavior of the porous metal foam truncated conical shell. In addition, using the quasi-3D theory, Zenkour et al.

*Corresponding author. *E-mail address:* hungpht@hcmute.edu.vn (Hung, P. T.)

[11, 12] analytically solved the bending of FG and FG sandwich porous plates. Nguyen et al. [13] utilized the polygonal finite element formulation to study the active vibration control of FG porous metal foam plates with GPL reinforcement.

From the literature reviews above, it is evident that numerous studies have focused on the behaviors of metal foam structures using analytical methods. Nonetheless, these techniques are limited to addressing straightforward problems with uncomplicated boundaries. For practical real-world structures, numerical methods like FEM, isogeometric analysis, and meshfree methods are preferred. In addition, Hung et al. [14] studied the buckling and dynamic of the porous metal foam plates according to the higher-order shear deformation theory (HSDT) with seven variables and moving Kriging meshfree method. Hughes et al. [15] pioneered the introduction of isogeometric analysis (IGA) utilizing NURBS functions. Throughout this decade, numerous researchers have effectively employed IGA for both plates and microplates. Phung-Van et al. [16] studied the nonlinear transient of the porous FGM plates using IGA. Besides, the free vibration, bending and dynamic control of the piezoelectric plates using the combination of HSDT and IGA were presented in ref. [17]. Lieu et al. [18] employed IGA to examine the free vibration of the FG porous plate with GPL reinforcement. The free vibration of the mutidirectional FG plates using IGA was investigated by Son et al. [19, 20]. Based on the Quasi-3D theory and modified couple stress theory, Thai et al. [21] investigated the buckling and free vibration of the multilayer FG plates reinforced with graphene platelets (GPLRC). Thai et al. [22] used the MSGT, HSDT and IGA to study the free vibration of the multilayer FG GPLRC microplates. Currently, there is a lack of research utilizing IGA based on Quasi-3D refined theory to investigate the effects of porosity properties on the frequency of porous metal foam plates resting on a Winkler-Pasternak foundation. This article address this gap by constructing a numerical model for metal foam plates characterized by symmetric, asymmetric and uniform porous distributions. The impact of the porous coefficient, porous distribution and geometry on the behavior of the metal foam plate presented.

2. The fundamental equations

2.1. The effective material properties

Let's contemplate porous metal foam plates with pores distributed throughout thickness of the plate in three manners: uniform (P-I), symmetric (P-II), and asymmetric (P-III). The porous metal foam plate and porosity distributions are shown in Fig. 1. The material properties of these microplates are outlined as follows [23]

P-I

$$\begin{cases} E(z) = E_1(1 - e_0\zeta) \\ G(z) = G_1(1 - e_0\zeta) \\ \rho(z) = \rho_1\left(1 - \sqrt{1 - e_0\zeta}\right) \\ \zeta = \dfrac{1}{e_0} - \dfrac{1}{e_0}\left(\dfrac{2}{\pi}\sqrt{1 - e_0} - \dfrac{2}{\pi} + 1\right)^2 \end{cases}$$

P-II

$$\begin{cases} E(z) = E_1\left[1 - e_0\cos\left(\dfrac{\pi z}{h}\right)\right] \\ G(z) = G_1\left[1 - e_0\cos\left(\dfrac{\pi z}{h}\right)\right] \\ \rho(z) = \rho_1\left[1 - e_m\cos\left(\dfrac{\pi z}{h}\right)\right] \end{cases} \tag{1}$$

P-III

$$\begin{cases} E(z) = E_1\left[1 - e_0\cos\dfrac{\pi}{4}\left(\dfrac{2z}{2h} + 1\right)\right] \\ G(z) = G_1\left[1 - e_0\cos\dfrac{\pi}{4}\left(\dfrac{2z}{h} + 1\right)\right] \\ \rho(z) = \rho_1\left[1 - e_m\cos\dfrac{\pi}{4}\left(\dfrac{2z}{h} + 1\right)\right] \end{cases}$$

in which

$$e_m = 1 - \sqrt{1 - e_0} \tag{2}$$

where e_m and e_0 are respectively denote the density porosity and porous coefficients. It is important to note that this study does not consider the local effects of pores. The description of e_m and e_0 is provided bellow

$$\begin{cases} e_0 = 1 - \dfrac{E_2}{E_1} = 1 - \dfrac{G_2}{G_1}, & 0 < e_0 < 1 \\ e_m = 1 - \dfrac{\rho_2}{\rho_1}, & 0 < e_m < 1 \end{cases} \tag{3}$$

where E_1, G_1, ρ_1 and E_2, G_2, ρ_2 are respectively represent the maximum and minimum values of elastic modulus, shear modulus, and mass density of the plate.

Besides, based on [23], the Poisson's ratio ν is considered constant throughout the plate thickness.

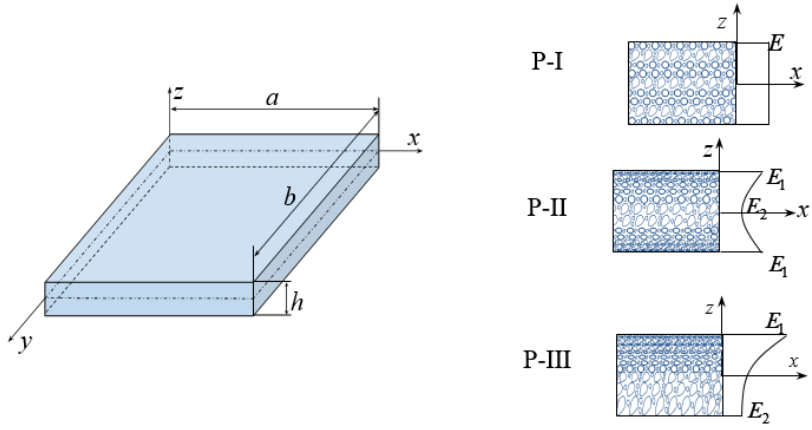

Figure 1. The porous metal foam plate

2.2. *The effective material properties*

Based on the Quasi-3D refined plate theory [24], the displacement fields are described as follows

$$\begin{cases} u = u_0 - zw_{b,x} + f(z)\, w_{s,x} \\ v = v_0 - zw_{b,y} + f(z)\, w_{s,y} \\ w = w_b + \phi(z)\, w_s \end{cases} \quad \text{with} \quad f(z) = z - \frac{4z^3}{3h^2}; \quad \phi(z) = \frac{1}{6}f'(z) \tag{4}$$

where u_0 and v_0 denote displacement of the middle surface, while wb and ws are respectively represent bending and shear deflection; the index "," denotes a differential operator.

The variational principle for free vibration of the porous plate resting on an elastic foundation is defined as follows

$$\delta U - \delta K - \delta W = 0 \tag{5}$$

where U, W and K represent the strain energy, work and kinetic energies, respectively.

The strain energy of the metal foam plate is described by

$$U = \int_V \boldsymbol{\varepsilon}^T \boldsymbol{\sigma} dV \tag{6}$$

where ε and σ represent the strain and Cauchy stress tensors, respectively.

The linear strain tensor of the porous plate is presented as follow

$$\boldsymbol{\varepsilon} = \frac{1}{2}\left[\nabla \mathbf{u} + (\nabla \mathbf{u})^T\right] \quad \text{with} \quad \nabla = \left\{ \begin{array}{ccc} \dfrac{\partial}{\partial x} & \dfrac{\partial}{\partial y} & \dfrac{\partial}{\partial z} \end{array} \right\} \tag{7}$$

where

$$\begin{gathered} \mathbf{u} = \left\{ \begin{array}{c} u \\ v \\ w \end{array} \right\} = \mathbf{u}_1 + z\mathbf{u}_2 + f(z)\,\mathbf{u}_3 + \phi(z)\,\mathbf{u}_4 \\ \mathbf{u}_1 = \left\{ \begin{array}{c} u_0 \\ v_0 \\ w_b \end{array} \right\}; \quad \mathbf{u}_2 = -\left\{ \begin{array}{c} w_{b,x} \\ w_{b,y} \\ 0 \end{array} \right\}; \quad \mathbf{u}_3 = \left\{ \begin{array}{c} w_{s,x} \\ w_{s,y} \\ 0 \end{array} \right\}; \quad \mathbf{u}_4 = \left\{ \begin{array}{c} 0 \\ 0 \\ w_s \end{array} \right\} \end{gathered} \tag{8}$$

After the substitution Eq. (8) into Eq. (7), the linear strain tensor is reformed as follows

$$\begin{gathered} \boldsymbol{\varepsilon} = \left\{ \begin{array}{c} \boldsymbol{\varepsilon}_b \\ \boldsymbol{\varepsilon}_s \end{array} \right\}; \quad \boldsymbol{\varepsilon}_b = \left\{ \begin{array}{c} \varepsilon_x \\ \varepsilon_y \\ \gamma_{xy} \\ \varepsilon_z \end{array} \right\} = \boldsymbol{\varepsilon}_{1b} + z\boldsymbol{\varepsilon}_{2b} + f(z)\,\boldsymbol{\varepsilon}_{3b} + \phi'(z)\,\boldsymbol{\varepsilon}_{4b} \\ \boldsymbol{\varepsilon}_s = \left\{ \begin{array}{c} \gamma_{xz} \\ \gamma_{yz} \end{array} \right\} = \left(f'(z) + \phi(z)\right)\boldsymbol{\gamma}_s \end{gathered} \tag{9}$$

where

$$\boldsymbol{\varepsilon}_{1b} = \left\{ \begin{array}{c} u_{0,x} \\ v_{0,y} \\ u_{0,y} + v_{0,x} \\ 0 \end{array} \right\}; \; \boldsymbol{\varepsilon}_{2b} = \left\{ \begin{array}{c} -w_{b,xx} \\ -w_{b,yy} \\ -2w_{b,xy} \\ 0 \end{array} \right\}; \; \boldsymbol{\varepsilon}_{3b} = \left\{ \begin{array}{c} w_{s,xx} \\ w_{s,yy} \\ 2w_{s,xy} \\ 0 \end{array} \right\}; \; \boldsymbol{\varepsilon}_{4b} = \left\{ \begin{array}{c} 0 \\ 0 \\ 0 \\ w_s \end{array} \right\}; \; \boldsymbol{\gamma}_s = \left\{ \begin{array}{c} w_{s,x} \\ w_{s,y} \end{array} \right\} \tag{10}$$

The stress-train relation based on the Hook law is presented by

$$\begin{gathered} \boldsymbol{\sigma}_b = \left\{ \begin{array}{c} \sigma_x \\ \sigma_y \\ \tau_{xy} \\ \sigma_z \end{array} \right\} = \left[\begin{array}{cccc} Q_{11} & Q_{12} & 0 & Q_{13} \\ Q_{12} & Q_{22} & 0 & Q_{23} \\ 0 & 0 & Q_{66} & 0 \\ Q_{13} & Q_{23} & 0 & Q_{33} \end{array} \right] \left\{ \begin{array}{c} \varepsilon_x \\ \varepsilon_y \\ \gamma_{xy} \\ \varepsilon_z \end{array} \right\} = \mathbf{C}_b \boldsymbol{\varepsilon}_b \\ \boldsymbol{\sigma}_s = \left\{ \begin{array}{c} \tau_{xz} \\ \tau_{yz} \end{array} \right\} = \left[\begin{array}{cc} Q_{55} & 0 \\ 0 & Q_{44} \end{array} \right] \left\{ \begin{array}{c} \gamma_{xz} \\ \gamma_{yz} \end{array} \right\} = \mathbf{C}_s \boldsymbol{\varepsilon}_s \end{gathered} \tag{11}$$

in which

$$\begin{gathered} Q_{11} = Q_{22} = Q_{33} = \frac{(1-\nu)E(z)}{(1-2\nu)(1+\nu)}; \quad Q_{13} = Q_{23} = Q_{12} = \frac{\nu E(z)}{(1-2\nu)(1+\nu)} \\ Q_{66} = Q_{55} = Q_{44} = \frac{E(z)}{2(1+\nu)} \end{gathered} \tag{12}$$

Substituting $\boldsymbol{\sigma}_b$ and $\boldsymbol{\sigma}_s$ in Eq. (9), into Eq. (6), the virtual strain energy is reformed by following

$$\delta U = \int_\Omega \delta\bar{\boldsymbol{\varepsilon}}_b^T \bar{\mathbf{D}}_b \bar{\boldsymbol{\varepsilon}}_b d\Omega + \int_\Omega \delta\boldsymbol{\gamma}_s^T \bar{\mathbf{D}}_s \boldsymbol{\gamma}_s d\Omega \tag{13}$$

where

$$\begin{gathered}\bar{\boldsymbol{\varepsilon}}_b = \left\{ \begin{array}{cccc} \varepsilon_{b1} & \varepsilon_{b2} & \varepsilon_{b3} & \varepsilon_{b4} \end{array} \right\}^T; \quad \bar{\mathbf{D}}_b = \begin{bmatrix} \mathbf{A} & \mathbf{B} & \mathbf{C} & \mathbf{E} \\ \mathbf{B} & \mathbf{D} & \mathbf{F} & \mathbf{L} \\ \mathbf{C} & \mathbf{F} & \mathbf{H} & \mathbf{O} \\ \mathbf{E} & \mathbf{L} & \mathbf{O} & \mathbf{P} \end{bmatrix} \\ (\mathbf{A}, \mathbf{B}, \mathbf{C}, \mathbf{E}, \mathbf{D}, \mathbf{F}, \mathbf{L}, \mathbf{H}, \mathbf{O}, \mathbf{P}) = \int_{-h/2}^{h/2} \left(1, z, f, \phi', z^2, zf, z\phi', f^2, f\phi', \phi'^2\right) \mathbf{C}_b dz \\ \bar{\mathbf{D}}_s = \int_{-h/2}^{h/2} (f' + \phi)^2 \, \mathbf{C}_s dz \end{gathered} \tag{14}$$

The expression for virtual kinetic energy can be expressed as follow

$$\delta K = \int_\Omega \delta\bar{\mathbf{u}}^T \mathbf{I}_m \ddot{\bar{\mathbf{u}}} d\Omega \tag{15}$$

in which

$$\begin{gathered}\bar{\mathbf{u}} = \left\{ \begin{array}{c} \mathbf{u}_1 \\ \mathbf{u}_2 \\ \mathbf{u}_3 \\ \mathbf{u}_4 \end{array} \right\}; \quad \mathbf{I}_m = \begin{bmatrix} \mathbf{I}_0 & 0 & 0 \\ 0 & \mathbf{I}_0 & 0 \\ 0 & 0 & \mathbf{I}_0 \end{bmatrix}; \quad \mathbf{I}_0 = \begin{bmatrix} A_m & B_m & C_m & E_m \\ B_m & D_m & F_m & L_m \\ C_m & F_m & H_m & O_m \\ E_m & L_m & O_m & P_m \end{bmatrix} \\ (A_m, B_m, C_m, E_m, D_m, F_m, L_m, H_m, O_m, P_m) = \int_{-h/2}^{h/2} \rho \left(1, z, f, \phi, z^2, zf, z\phi, f^2, f\phi, \phi^2\right) dz \end{gathered} \tag{16}$$

The virtual work performed by an elastic foundation can be represented as follows

$$\delta W = -\int_\Omega \left(k_w w - k_s \nabla^2 w\right) \delta w d\Omega \tag{17}$$

in which k_w and k_s are respectively represent the spring and shear coefficients of the foundation.

Substituting Eqs. (13), (15) and (17) into Eq. (5), the weak form of the porous metal foam plates is reformed by

$$\begin{gathered}\int_\Omega \delta\bar{\boldsymbol{\varepsilon}}_b^T \bar{\mathbf{D}}_b \bar{\boldsymbol{\varepsilon}}_b d\Omega + \int_\Omega \delta\boldsymbol{\gamma}_s^T \bar{\mathbf{D}}_s \boldsymbol{\gamma}_s d\Omega + \int_\Omega \delta\bar{\mathbf{u}}^T \mathbf{I}_m \ddot{\bar{\mathbf{u}}} d\Omega \\ - \int_\Omega \left[k_w w - k_s \nabla^2 w\right] \delta w d\Omega = \mathbf{0} \end{gathered} \tag{18}$$

2.3. NURBs approximation

In two dimensions (2D), NURBS basis functions [15] are defined using two knot vectors, $\bar{\mathbf{U}} = \left\{\eta_1, \eta_2, \ldots, \eta_{n+p+1}\right\}$ and $\bar{\mathbf{V}} = \left\{\zeta_1, \zeta_2, \ldots, \zeta_{m+q+1}\right\}$. Here, n and m represent the number of control points in the respective directions, while p and q correspond to the polynomial orders. The computation of the basis functions for 2D B-splines includes:

$$N_{i,j}(\eta, \zeta) = \widehat{N}_{i,p}(\eta) \, \widehat{M}_{j,q}(\zeta) \tag{19}$$

The B-spline basis functions $\widehat{N}$ and $\widehat{M}$ are generated using the Cox-de Boor algorithm, as outlined as follows

$$\begin{aligned}\widehat{M}_{j,0}(\zeta) &= \begin{cases} 1 & \text{if } \zeta_j \le \zeta \le \zeta_{j+1} \\ 0 & \text{otherwise} \end{cases} \qquad (q=0) \\ \widehat{N}_{i,0}(\eta) &= \begin{cases} 1 & \text{if } \eta_i \le \eta \le \eta_{i+1} \\ 0 & \text{otherwise} \end{cases} \qquad (p=0)\end{aligned} \tag{20}$$

and

$$\begin{aligned}\widehat{M}_{j,q}(\zeta) &= \frac{\zeta-\zeta_j}{\zeta_{j+q}-\zeta_j}\widehat{M}_{j,q-1}(\zeta) + \frac{\zeta_{j+q+1}-\zeta}{\zeta_{j+q+1}-\zeta_{j+1}}\widehat{M}_{j+1,q-1}(\zeta) \qquad (q \ge 1) \\ \widehat{N}_{i,p}(\eta) &= \frac{\eta-\eta_i}{\eta_{i+p}-\eta_i}\widehat{N}_{i,p-1}(\eta) + \frac{\eta_{i+p+1}-\eta}{\eta_{i+p+1}-\eta_{i+1}}\widehat{N}_{i+1,p-1}(\eta) \qquad (p \ge 1)\end{aligned} \tag{21}$$

NURBS basis functions are derived by combining the B-spline basis functions with their respective weights, as demonstrated below

$$N_{i,j}(\eta,\zeta) = N_e(\kappa) = \frac{\widehat{N}_{i,p}(\eta)\,\widehat{M}_{j,q}(\zeta)\,w_{i,j}}{\sum_{\hat{i}=1}^{n}\sum_{\hat{j}=1}^{m}\widehat{N}_{\hat{i},p}(\eta)\,\widehat{M}_{\hat{j},q}(\zeta)\,w_{\hat{i},\hat{j}}} \tag{22}$$

The displacement fields according to the NURBS basic functions in Eq. (22) are approximated by

$$\mathbf{u}^h(x,y) = \sum_{e=1}^{m\times n}\mathbf{N}_e(x,y)\,\mathbf{d}_e \quad \text{with} \quad \mathbf{N}_e(x,y) = \begin{bmatrix} N_e(x,y) & 0 & 0 & 0 \\ 0 & N_e(x,y) & 0 & 0 \\ 0 & 0 & N_e(x,y) & 0 \\ 0 & 0 & 0 & N_e(x,y) \end{bmatrix} \tag{23}$$

where $N_e(x,y)$ is NURBs basic function.

The strain tensor after the substituting Eq. (23) into Eq. (10), is reformed as follows

$$\bar{\boldsymbol{\varepsilon}}_b = \sum_{e=1}^{m\times n}\begin{Bmatrix} \mathbf{B}_{1e}^b & \mathbf{B}_{2e}^b & \mathbf{B}_{3e}^b & \mathbf{B}_{4e}^b \end{Bmatrix}^T \mathbf{d}_e = \sum_{e=1}^{m\times n}\bar{\mathbf{B}}_{be}\mathbf{d}_e; \quad \boldsymbol{\gamma}_s = \sum_{e=1}^{m\times n}\bar{\mathbf{B}}_{se}\mathbf{d}_e \tag{24}$$

in which

$$\begin{aligned}\mathbf{B}_{1e}^b &= \begin{bmatrix} N_{e,x} & 0 & 0 & 0 \\ 0 & N_{e,y} & 0 & 0 \\ N_{e,y} & N_{e,x} & 0 & 0 \\ 0 & 0 & 0 & 0 \end{bmatrix}; \quad \mathbf{B}_{2e}^b = \begin{bmatrix} 0 & 0 & -N_{e,xx} & 0 \\ 0 & 0 & -N_{e,yy} & 0 \\ 0 & 0 & -2N_{e,xy} & 0 \\ 0 & 0 & 0 & 0 \end{bmatrix}; \quad \mathbf{B}_{3e}^b = \begin{bmatrix} 0 & 0 & 0 & N_{e,xx} \\ 0 & 0 & 0 & N_{e,yy} \\ 0 & 0 & 0 & 2N_{e,xy} \\ 0 & 0 & 0 & 0 \end{bmatrix}; \\ \mathbf{B}_{4e}^b &= \begin{bmatrix} 0 & 0 & 0 & 0 \\ 0 & 0 & 0 & 0 \\ 0 & 0 & 0 & 0 \\ 0 & 0 & 0 & N_e \end{bmatrix}; \quad \mathbf{B}_{se} = \begin{bmatrix} 0 & 0 & 0 & N_{e,x} \\ 0 & 0 & 0 & N_{e,y} \end{bmatrix}\end{aligned} \tag{25}$$

In addition, the displacement vector $\bar{u}$ can be reformed as follows

$$\bar{\mathbf{u}} = \sum_{e=1}^{m\times n}\begin{Bmatrix} \mathbf{N}_{1e} & \mathbf{N}_{2e} & \mathbf{N}_{3e} & \mathbf{N}_{4e} \end{Bmatrix}^T \mathbf{d}_e = \sum_{e=1}^{m\times n}\bar{\mathbf{N}}_e\mathbf{d}_e \tag{26}$$

where

$$\mathbf{d}_e = \left\{ \begin{array}{cccc} u_{0e} & v_{0e} & w_{be} & w_{se} \end{array} \right\}^T$$

$$\mathbf{N}_{1e} = \begin{bmatrix} N_e & 0 & 0 & 0 \\ 0 & N_e & 0 & 0 \\ 0 & 0 & N_e & 0 \end{bmatrix}; \quad \mathbf{N}_{2e} = \begin{bmatrix} 0 & 0 & -N_{e,x} & 0 \\ 0 & 0 & -N_{e,y} & 0 \\ 0 & 0 & 0 & 0 \end{bmatrix}$$

$$\mathbf{N}_{3e} = \begin{bmatrix} 0 & 0 & 0 & N_{e,x} \\ 0 & 0 & 0 & N_{e,y} \\ 0 & 0 & 0 & 0 \end{bmatrix}; \quad \mathbf{N}_{4e} = \begin{bmatrix} 0 & 0 & 0 & 0 \\ 0 & 0 & 0 & 0 \\ 0 & 0 & 0 & N_e \end{bmatrix} \tag{27}$$

The weak form for vibration behavior of the metal foam plate is presented by

$$\left(\mathbf{K} + \mathbf{K}_f - \omega^2 \mathbf{M}\right) \bar{\mathbf{d}} = 0 \tag{28}$$

where $\mathbf{K}$ and $\mathbf{M}$ respectively denote the global stiffness and mass matrices, as expressed below

$$\begin{gathered} \mathbf{K} = \int_\Omega \bar{\mathbf{B}}_b^T \bar{\mathbf{D}}_b \bar{\mathbf{B}}_b d\Omega + \int_\Omega \bar{\mathbf{B}}_s^T \bar{\mathbf{D}}_s \mathbf{B}_s d\Omega; \quad \mathbf{K}_f \int_\Omega \mathbf{B}_f^T \left(k_w \mathbf{B}_f - k_s \nabla^2 \mathbf{B}_f\right) d\Omega \\ \mathbf{M} = \int_\Omega \bar{\mathbf{N}}^T \mathbf{I}_m \bar{\mathbf{N}} d\Omega; \quad \mathbf{B}_f = \left\{ \begin{array}{cccc} 0 & 0 & N_e & hN_e/9 \end{array} \right\}; \quad \mathbf{d} = \bar{\mathbf{d}} \mathrm{e}^{i\omega t} \end{gathered} \tag{29}$$

where ω, $\bar{\mathbf{d}}$ respectively represent natural frequency and mode shapes.

3. Numerical results

Let's examine rectangular plates made of porous metal foam, with length a, width b and thickness h. The material properties are obtained from [25] as follows: $E_1 = 200\,\mathrm{GPa}, \nu_1 = 0.33, \rho_1 = 7850\,\mathrm{kg/m^3}$. For numerical examples, the plate is modeled using an 11×11 meshes grid. The boundary conditions (BCs) are applied as follows

- Fully simply supported (SSSS): $(v_0, w_b, w_s)|_{x=0,a} = 0$; $(u_0, w_b, w_s)|_{x=0,a} = 0$.
- Fully clamped (CCCC): $(u_0, v_0, w_b, w_s, w_{b,n}, w_{s,n})\big|_{x=0,a;y=0,b} = 0$.
- Simply supported at $y = 0, b$ and clamped at $x = 0, a$ (SCSC): $(u_0, w_b, w_s)|_{y=0,b} = 0$; $(u_0, v_0, w_b, w_s, w_{b,n}, w_{s,n})_{x=0,a} = 0$.

The following dimensionless natural frequency and spring and shear coefficients of the FG plates are presented as follows

$$\bar{\omega} = \omega h \sqrt{\rho_m / E_m}; \quad \bar{K}_w = a^4 k_w / D_m; \quad \bar{K}_s = a^2 k_s / D_m; \quad D_m = \frac{E_m h^3}{12\left(1 - \nu_m^2\right)} \tag{30}$$

For the metal foam plate, the dimensionless natural frequency and spring and shear coefficients are taken by

$$\Omega = 100\omega h \sqrt{\rho_1 / E_1}; \quad K_w = a^4 k_w / D; \quad K_s = a^2 k_s / D; \quad D = \frac{E_1 h^3}{12\left(1 - \nu_1^2\right)} \tag{31}$$

Firstly, the free vibration of the FG plate made of Al/ZrO_2 with the material properties are taken from [26], is examined. The first dimensioless natural frequency $\bar{\omega}$ of the FG plate resting on elastic foundation is tabulated in Table 1. The results are compared with those given by Alazwari et al. [26] using the Quasi-3D theory and analytical method. According to the data in Table 1, the present results are in good agreement with the reference's results. Next, the first normalized vibrational

frequencies Ω of the SSSS porous rectangular plates with different values of the parameters e_0 and b/a are examined and tabulated in Table 2. The results of the present study are compared with the reference solution provided by Hung et al. [25] using the refined plate theory and IGA. We can see from Table 2, that the results are matched very well with the published results. The comparison results in Table 1 and Table 2 demonstrate that the proposed method is accurate and consistent to investigate the free vibration of the porous metal foam plates.

Table 1. The first dimensionless frequency of the SSSS FG square plate with various power indexes ($a/h = 5$)

$\bar{K}_w$	$\bar{K}_s$	n					
		2		3		5	
		Present	Ref. [26]	Present	Ref. [26]	Present	Ref. [26]
0	0	0.2285	0.22848	0.2292	0.22901	0.2299	0.22952
10	0	0.2307	0.23062	0.2315	0.23130	0.2323	0.23199
10	10	0.2697	0.26937	0.2730	0.27256	0.2766	0.27610

Table 2. The first non-dimensional frequencies of the SSSS porous rectangular plates with various thickness-to-width ratios ($a/h = 10, e_0 = 0.2, K_w = 0, K_s = 0$)

Porosity distribution	e_0	b/a					
		1		2		3	
		Present	Ref. [25]	Present	Ref. [25]	Present	Ref. [25]
P-I	0.1	5.7395	5.7276	3.6317	3.6268	3.2357	3.2318
	0.2	5.6361	5.6244	3.5663	3.5615	3.1774	3.1736
	0.3	5.5239	5.5125	3.4953	3.4906	3.1142	3.1104
P-II	0.1	5.8157	5.8052	3.6820	3.6777	3.2809	3.2774
	0.2	5.7999	5.7905	3.6743	3.6704	3.2744	3.2713
	0.3	5.7898	5.7806	3.6704	3.6667	3.2714	3.2684
P-III	0.1	5.7544	5.7422	3.6415	3.6363	3.2445	3.2404
	0.2	5.6668	5.6527	3.5864	3.5800	3.1955	3.1902
	0.3	5.5711	5.5529	3.5262	3.5169	3.1419	3.1340

Table 3. The first six non-dimensional natural frequencies of the porous square plate with various porosity coefficients ($a/h = 10, K_w = 20, K_s = 2$)

BCs	Mode	e_0					
		0.1	0.2	0.3	0.4	0.5	0.6
SSSS	1	6.2076	6.1290	6.0457	5.9568	5.8612	5.7575
	2	14.0963	13.8707	13.6277	13.3632	13.0719	12.7452
	3	14.0963	13.8707	13.6277	13.3632	13.0719	12.7452
	4	18.9451	18.6038	18.2334	17.8268	17.3739	16.8588
	5	21.4240	21.0653	20.6778	20.2548	19.7867	19.2589
	6	26.0387	25.5966	25.1186	24.5963	24.0176	23.3639

BCs	Mode	e_0					
		0.1	0.2	0.3	0.4	0.5	0.6
CCCC	1	11.1434	10.9642	10.7711	10.5609	10.3291	10.0691
	2	20.6769	20.3262	19.9470	19.5327	19.0736	18.5552
	3	20.6769	20.3262	19.9470	19.5327	19.0736	18.5552
	4	28.6271	28.1340	27.6003	27.0164	26.3686	25.6357
	5	33.6431	33.0598	32.4283	31.7372	30.9699	30.1012
	6	33.7792	33.1931	32.5583	31.8637	31.0924	30.2190

Table 4. The effect of the various porosity distribution and parameter a/h on the first six non-dimensional frequencies of the porous square plate ($e_0 = 0.2, K_w = 20, K_s = 2$)

Mode	SSSS			CCCC		
	a/h					
	10	20	30	10	20	30
			P-I			
1	6.1290	1.5676	0.6998	10.9642	2.8387	1.2625
2	13.8707	3.6674	1.6487	20.3262	5.5598	2.5050
3	13.8707	3.6674	1.6487	20.3262	5.5598	2.5050
4	21.0653	5.7316	2.5939	28.1340	7.9827	3.6346
5	25.5966	7.0853	3.2202	33.0598	9.5821	4.3899
6	25.5966	7.0853	3.2202	33.1931	9.6428	4.4153
			P-II			
1	6.2798	1.6097	0.7189	11.2649	2.9211	1.2998
2	14.1978	3.7725	1.6979	20.8226	5.7218	2.5806
3	14.1978	3.7725	1.6979	20.8226	5.7218	2.5806
4	21.5103	5.8928	2.6714	28.7304	8.2098	3.7438
5	26.0984	7.2807	3.3160	33.7012	9.8497	4.5211
6	26.0984	7.2807	3.3160	33.8470	9.9123	4.5472
			P-III			
1	6.1572	1.5754	0.7033	11.0192	2.8535	1.2692
2	13.9330	3.6870	1.6578	20.4200	5.5893	2.5187
3	13.9330	3.6870	1.6578	20.4200	5.5893	2.5187
4	21.1518	5.7618	2.6083	28.2505	8.0245	3.6545
5	25.6956	7.1220	3.2380	33.1875	9.6315	4.4139
6	25.6956	7.1220	3.2380	33.3240	9.6927	4.4394

Moving forward, the effect of the porosity coefficient, porous distribution and geometry on the free vibration of the porous metal foam square plates is examined. The impact of the porous coefficient on the lowest six frequencies of the uniform porous square plate is presented in Table 3. According to the results in Table 3, an increase in the porous coefficient leads to a decrease in the non-dimensional frequencies of the metal foam plates. Table 4 shows the porous plate's first six nor-

Table 5. The effect of the length-to-width ratio on the first six non-dimensional frequencies of the porous rectangular plate ($e_0 = 0.1, K_w = 20, K_s = 2$)

BCs	Mode	a/b				
		1	1.5	2	2.5	3
SSSS	1	6.2780	4.4220	3.7764	3.4798	3.3195
	2	14.2484	8.1376	5.9050	4.8540	4.2783
	3	14.2484	12.5847	9.3466	7.0987	5.8538
	4	21.6307	14.0239	12.0046	10.1545	8.0167
	5	26.2716	15.9938	13.9491	11.7367	10.7383
	6	26.2716	21.4189	13.9637	12.9894	11.5914
CCCC	1	11.2836	8.5201	7.7769	7.4954	7.3622
	2	20.9078	12.5185	9.7532	8.6212	8.0760
	3	20.9078	18.8806	13.2055	10.6686	9.3874
	4	28.9041	18.9530	17.9622	13.6448	11.3525
	5	33.9406	22.1952	18.3791	17.4716	13.9677
	6	34.0827	26.9959	20.0631	18.1389	17.2200

malized vibrational frequencies with various porous distributions and length-to-thickness ratios. It can be seen from Table 4 that with a rise in the length-to-thickness ratio, the frequencies of the porous plates rise as well. The influence of the width-to-length ratio on the first six dimensionless natural frequency of the metal foam restangular plates is also exmined and shown in Table 5. With an increase of the width-to-length ratio, the natural frequency decreases. Moreover, the symmetric distribution offers the highest natural frequency among the porosity distributions, followed by asymmetric and uniform distributions. Fig. 2 and Fig. 3 respectively plot the first normalized natural frequency Ω of the asymmetric porous metal foam plate with various values of spring and shear coefficients of a elastic foundation. As shown in Fig. 2, and Fig. 3 an increase in the spring and shear coefficients leads to a decrease in the vibrational frequency of the porous plate. In addition, among the boundary conditions, the CCCC boundaries provide the highest frequency, while the SSSS boundaries provide the smallest frequency.

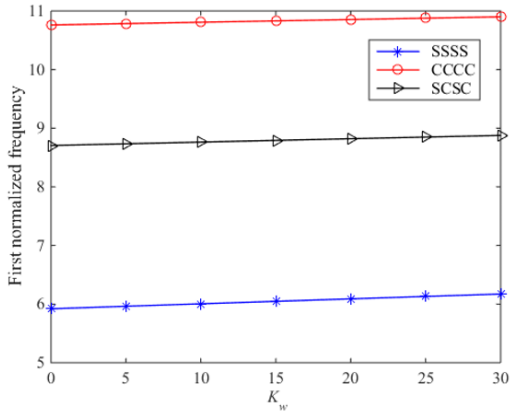

Figure 2. The first dimensionless natural frequency of the metal foam plate with various values of K_w and BCs (P-III, $a/h = 10, e_0 = 0.3, K_s = 2$)

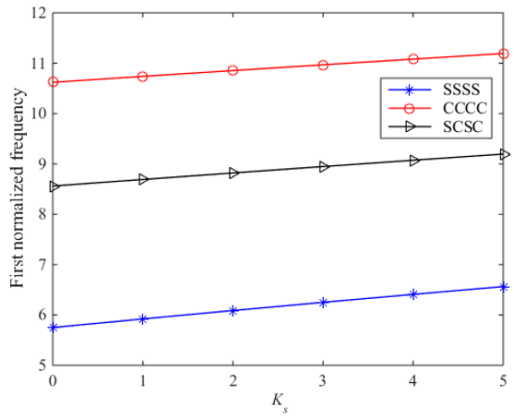

Figure 3. The first dimensionless natural frequency of the metal foam plate with various values of K_s and BCs (P-III, $a/h = 10, e_0 = 0.3, K_w = 20$)

4. Conclusions

In this study, the free vibration of porous metal foam plates with uniform, symmetric, and asymmetric porosity distributions is studied using IGA and Quasi-3D refined theory with four variables. The explicit governing equations of the plate are derived based on variational principles. The study examines the influence of pore distribution, length-to-thickness ratio, and boundary conditions on the natural frequency of the metal foam plates. The results indicate that a rise in the length-to-thickness and width-to-length ratios leads to smaller natural frequencies of the porous plates. Additionally, the plate's stiffness decreases with a higher porosity coefficient. Between the porosity distribution, symmetric distribution provides the highest stiffness, while the uniform distribution provides the smallest. An increse of the spring and shear coefficients of a Winkler-Pasternak foundation make the natural frequency of the metal foam plates rise.

Acknowledgements

This work belongs to the project in 2025 funded by Ho Chi Minh City University of Technology and Education, Vietnam.

References

[1] Chen, D., Kitipornchai, S., Yang, J. (2016). Nonlinear free vibration of shear deformable sandwich beam with a functionally graded porous core. *Thin-Walled Structures*, 107:39–48.

[2] Jabbari, M., Hashemitaheri, M., Mojahedin, A., Eslami, M. (2014). Thermal buckling analysis of functionally graded thin circular plate made of saturated porous materials. *Journal of Thermal Stresses*, 37 (2):202–20.

[3] Jabbari, M., Mojahedin, A., Khorshidvand, A. R., Eslami, M. R. (2014). Buckling analysis of a functionally graded thin circular plate made of saturated porous materials. *Journal of Engineering Mechanics*, 140(2):287–295.

[4] Barati, M. R., Shahverdi, H., Zenkour, A. M. (2017). Electro-mechanical vibration of smart piezoelectric FG plates with porosities according to a refined four-variable theory. *Mechanics of Advanced Materials and Structures*, 24(12):987–98.

[5] Keddouri, A., Hadji, L., Tounsi, A. (2019). Static analysis of functionally graded sandwich plates with porosities. *Advances in Materials Research*, 8(3):155–77.

[6] Ebrahimi, F., Dabbagh, A., Rastgoo, A. (2019). Vibration analysis of porous metal foam shells rested on an elastic substrate. *The Journal of Strain Analysis for Engineering Design*, 54(3):199–208.

[7] Rezaei, A., Saidi, A., Abrishamdari, M., Mohammadi, M. P. (2017). Natural frequencies of functionally graded plates with porosities via a simple four variable plate theory: An analytical approach. *Thin-Walled Structures*, 120:366–377.

[8] Wang, Y. Q., Ye, C., Zu, J. W. (2019). Nonlinear vibration of metal foam cylindrical shells reinforced with graphene platelets. *Aerospace Science and Technology*, 85:359–370.

[9] Ebrahimi, F., Dabbagh, A., Taheri, M. (2021). Vibration analysis of porous metal foam plates rested on viscoelastic substrate. *Engineering with Computers*, 37(4):3727–39.

[10] Li, H., Hao, Y., Zhang, W., Liu, L., Yang, S., Wang, D. (2021). Vibration analysis of porous metal foam truncated conical shells with general boundary conditions using GDQ. *Composite Structures*, 269: 114036.

[11] Zenkour, A. M. (2018). A quasi-3D refined theory for functionally graded single-layered and sandwich plates with porosities. *Composite Structures*, 201:38–48.

[12] Zenkour, A. M. (2020). Quasi-3D refined theory for functionally graded porous plates: displacements and stresses. *Physical Mesomechanics*, 23(1):39–53.

[13] Nguyen, N. V., Lee, J., Nguyen-Xuan, H. (2019). Active vibration control of GPLs-reinforced FG metal foam plates with piezoelectric sensor and actuator layers. *Composites Part B: Engineering*, 172:769–784.

[14] Hung, P. T., Thai, C. H., Phung-Van, P. (2022). A moving Kriging meshfree approach for free vibration and buckling analyses of porous metal foam plates. *Journal of Micromechanics and Molecular Physics*, 8(01):45–59.

[15] Hughes, T. J. R., Cottrell, J. A., Bazilevs, Y. (2005). Isogeometric analysis: CAD, finite elements, NURBS, exact geometry and mesh refinement. *Computer Methods in Applied Mechanics and Engineering*, 194(39–41):4135–4195.

[16] Phung-Van, P., Thai, C. H., Ferreira, A. J. M., Rabczuk, T. (2020). Isogeometric nonlinear transient analysis of porous FGM plates subjected to hygro-thermo-mechanical loads. *Thin-Walled Structures*, 148:106497.

[17] Phung-Van, P., De Lorenzis, L., Thai, C. H., Abdel-Wahab, M., Nguyen-Xuan, H. (2015). Analysis of laminated composite plates integrated with piezoelectric sensors and actuators using higher-order shear deformation theory and isogeometric finite elements. *Computational Materials Science*, 96:495–505.

[18] Nguyen, L. B., Viet, T. B., Nguyen, H.-Y. (2021). An isogeometric formulation with a three-variable high order shear deformation theory for free vibration analysis of FG porous plates reinforced by graphene platelets. *Journal of Science and Technology in Civil Engineering (JSTCE)-HUCE*, 15(2):51–66.

[19] Son, T., Qui, L. X. (2022). Investigate the bending and free vibration responses of multi-directional functionally graded plates with variable thickness based on isogeometric analysis. *Journal of Science and Technology in Civil Engineering (JSTCE)-HUCE*, 16(4):10–29.

[20] Son, T., Huu-Tai, T. (2019). Free-vibration analysis of multi-directional functionally graded plates based on 3D isogeometric analysis. *Journal of Science and Technology in Civil Engineering (JSTCE)-HUCE*, 13(2):1–11.

[21] Thai, C. H., Ferreira, A. J. M., Tran, T. D., Phung-Van, P. (2020). A size-dependent quasi-3D isogeometric model for functionally graded graphene platelet-reinforced composite microplates based on the modified couple stress theory. *Composite Structures*, 234:111695.

[22] Thai, C. H., Ferreira, A. J. M., Phung-Van, P. (2019). Size dependent free vibration analysis of multilayer functionally graded GPLRC microplates based on modified strain gradient theory. *Composites Part B: Engineering*, 169:174–188.

[23] Barati, M. R. (2017). Nonlocal-strain gradient forced vibration analysis of metal foam nanoplates with uniform and graded porosities. *Advances in Nano Research*, 5(4):393.

[24] Thai, C. H., Zenkour, A. M., Wahab, M. A., Nguyen-Xuan, H. (2016). A simple four-unknown shear and normal deformations theory for functionally graded isotropic and sandwich plates based on isogeometric analysis. *Composite Structures*, 139:77–95.

[25] Pham-Tan, H., Thai, C. H., Phung-Van, P. (2022). NURBS-based refined plate theory for metal foam plates with porosities. *Thin-Walled Structures*, 175:109246.

[26] Alazwari, M. A., Zenkour, A. M. (2022). A Quasi-3D Refined Theory for the Vibration of Functionally Graded Plates Resting on Visco-Winkler-Pasternak Foundations. *Mathematics*, 10(5):716.